Insights into cation disorder and phase transitions in CZTS from a first-principles approach

S. P. Ramkumar, A. Miglio, M. J. van Setten, D. Waroquiers, G. Hautier, and G.-M. Rignanese
IMCN-NAPS, Université catholique de Louvain, Chemin des Étoiles 8, B-1348 Louvain-la-Neuve, Belgium and European Theoretical Spectroscopy Facility (ETSF)

(Received 23 May 2018; published 9 August 2018)

Cu_2ZnSnS_4 (CZTS) is a promising thin-film photovoltaic absorber material consisting of earth-abundant and nontoxic elements, though the efficiency achieved in actual devices is well below the theoretical one. Cation disorder has been proposed as a possible explanation; it is, however, still badly understood. A recent investigation based on high-resolution neutron diffraction experiments by Bosson *et al.* [J. Mater. Chem. A **5**, 16672 (2017)] contradicts previous reports and indicates Cu-Zn disorder, not just in the 2*c* and 2*d* Wyckoff sites but also in the 2*a* site of Cu. To clear up this confusion on the exact nature of the disorder, we employ a ternary cluster expansion in combination with Monte Carlo simulations to analyze the phase characteristics of CZTS while undergoing order-disorder transitions. Our calculations show that, in excellent agreement with experiments, a low-temperature phase transition takes place close to 545 K and that the nature of the corresponding disorder is the same as the one recently observed experimentally by Bosson *et al.*

DOI: 10.1103/PhysRevMaterials.2.085403

I. INTRODUCTION

As a consequence of the exponentially increasing energy demand, the depletion of fossil fuels, and the growing threat of climate change, renewable energy sources are becoming more and more important. Among these, solar energy is projected to play a dominant role [1]. During the last couple of decades, thin-film photovoltaic (PV) cells have gained popularity [2]. In thin-film PV technology, CdTe and $CuIn_xGa_{1-x}(S, Se)_2$ (CIGSSe) have been the commercially viable absorber materials so far, with efficiencies close to 21% [2].

The past few years have seen a growing interest in $Cu_2ZnSn(S, Se)_4$ (CZTSSe) arising out of sustainability and environmental concerns over Cd toxicity and scarcity of Te, In, and Ga. However, at present, these materials are not commercially competitive, as their efficiency (close to 12.6% [3] for CZTSSe and 8.6% [4] for CZTS) is far from that of more mature thin-film technologies. This low efficiency is attributed to a large deficit in the open-circuit voltage (V_{oc}), which reaches only about 60% of the theoretical maximum [5]. A number of hypotheses have been proposed to account for this low V_{oc}. First, it might result from the formation of secondary phases due to the narrow phase stability range of CZTS [6,7]. Another possible explanation is the presence of point defects in the material, especially arising from disorder in the Cu-Zn sublattice and tail states causing electrostatic potential fluctuations [8,9]. It has been found that the formation energies of Cu-Zn antisite defects are low while defects involving Sn require higher energies due to the size mismatch between Sn and Cu/Zn [10–14]. Cu-Zn disorder is hence dominating. Furthermore, disorder has been shown to affect the electronic properties of CZTS, leading to a decrease in the band gap, as observed in photoluminescence (PL) and derivation of absorption spectrum fitting (DASF) experiments [8,15,16]. The existence and importance of Cu-Zn disorder has been widely observed in several studies based on x-ray and neutron diffraction [17], theoretical and experimental Raman spectra [18–21], nuclear magnetic resonance (NMR) [22,23], and PL measurements [8].

Experimentally, CZTS is found to crystallize in the kesterite (KS) structure (with space group $I\bar{4}$) [17,24,25], illustrated in Fig. 1(a). Several theoretical studies [10,26] based on density functional theory (DFT) also found KS to be the most stable structure. It has alternating Cu/Zn and Cu/Sn planes along the [001] direction and four different cationic sites: one Cu is located at the Wyckoff position 2*a* (0,0,0), the other Cu at 2*c* (0,1/2,1/4), Zn at 2*d* (0,1/2,3/4), and Sn at 2*b* (0,0,1/2). Until recently, the common understanding, emerging from various experiments (e.g., Raman spectroscopy [18] and neutron powder diffraction [27]) was that above a critical temperature T_c (ranging from 533 to 552 K [18,27]), KS evolves into a phase with disorder in the Cu-2*c* and Zn-2*d* sites. This disorder phase is represented in Fig. 1(b) and will be denoted as Cu-Zn plane disordered (CZ-PD) [5]. However, more recent high-precision neutron diffraction experiments [14] indicate that cation disorder is not restricted to the 2*c* and 2*d* sites but extends to the 2*a* site, as illustrated in Fig. 1(c), contradicting the interpretation of all previous experimental results. This phase will be referred to as Cu-Zn fully disordered (CZ-FD). *In situ* high-temperature x-ray diffraction from synchrotron sources and neutron diffraction experiments [14,17,28] showed an additional structural phase transition from a tetragonal to a cubic phase close to 1150 K with a mixed phase present between 1139 and 1156 K. This high-temperature experimental phase formed due to loss of long-range order denotes an evolution to a complete cation disorder which is represented in Fig. 1(d) and will be denoted as the fully disordered (FD) phase.

Various theoretical studies have also been dedicated to the disorder in CZTS. Shang *et al.* [29] performed calculations based on special quasirandom structures (SQS) [30] considering disorder in the Cu-Zn planes only for a $2 \times 2 \times 1$ supercell

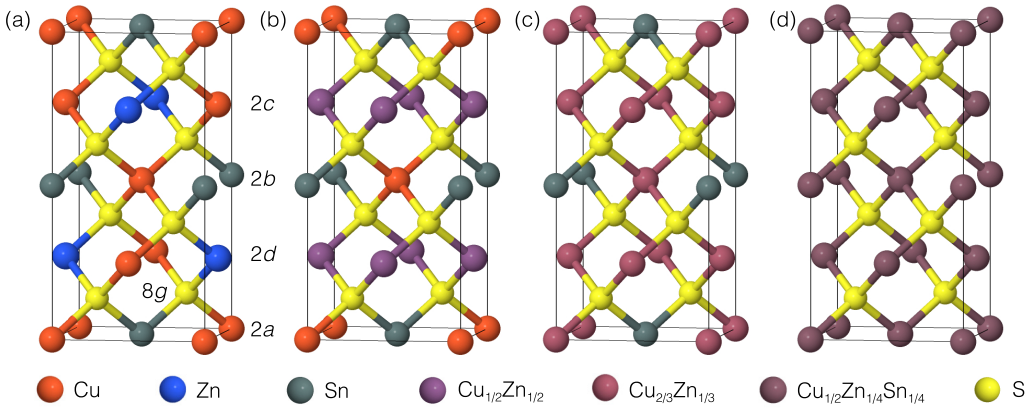

FIG. 1. Tetragonal unit cells of (a) KS, (b) Cu-Zn plane disordered (CZ-PD), (c) Cu-Zn fully disordered (CZ-FD), and (d) fully disordered (FD) phases.

of the ZnS eight-atom unit cell. Yu and Carter [31] considered disorder among all Cu-Zn sites by using a cluster expansion [32] (CE)-based Hamiltonian in combination with Monte Carlo simulations (MC) [33] in a $4 \times 4 \times 2$ supercell. Zawadzki *et al.* [34] considered a motif-based model Hamiltonian in combination with MC to describe the electronic properties of CZTS. In all cases, the critical temperature for the first order-disorder transition was found to be very close to the experimental observations. But the nature of the disorder could not be identified.

The aim of this paper is to provide a clear understanding of the nature of the disorder in CZTS. First, we identify the order-disorder transitions via a combined CE and MC approach. We then analyze the different phase characteristics and provide insight into the evolution of disorder in stoichiometric CZTS.

II. COMPUTATIONAL DETAILS

DFT calculations were performed with the VASP [35] code using the projector augmented wave (PAW) [36] method. We adopted the Perdew-Burke-Ernzerhof (PBE) exchange-correlation functional [37], including a Hubbard U correction (PBE+U) for the Cu-d states [38]. A U value of 6.0 eV was chosen in accordance with previous studies [39–43] in order to obtain accurate structural parameters (including the anion displacement) and electronic properties [44]. The atomic positions and lattice vectors were optimized with a convergence criterium on the total energy of 0.4 meV/atom and 50 meV/Å on the forces. For all these calculations, a kinetic energy cutoff of 520 eV was employed for truncating the plane-wave basis set. The Brillouin zone was sampled using a Γ-point centered k-point mesh with a density corresponding to 10 000 points per reciprocal atom (i.e., the number of points in the full Brillouin zone times the number of atoms equals 10 000).

Using the ATAT [45] package, a CE of the total energy was obtained based on the occupation of the four cationic sites of a ZnS eight-atom unit cell by either Cu, Zn, or Sn (see Appendix). The dominant interactions in the CE are found to involve only first and second nearest-neighbor cations, referred to as 1NN and 2NN, and three pair-correlation functions: f_0f_0 (f00), f_1f_0 (f10), and f_1f_1 (f11) (see Appendix). Based on this CE, MC simulations were performed using the MEMC2 code [46] in ATAT in a canonical ensemble, sampling the relevant microstates with the standard Metropolis algorithm. For these calculations, we used a $20 \times 20 \times 20$ supercell consisting of 64 000 atoms (i.e., 32 000 cationic active sites), significantly larger than those considered by Zawadzki *et al.* [34] and Yu *et al.* [31]. At each temperature, the system was first equilibrated by executing 10^6 passes and subsequently, the

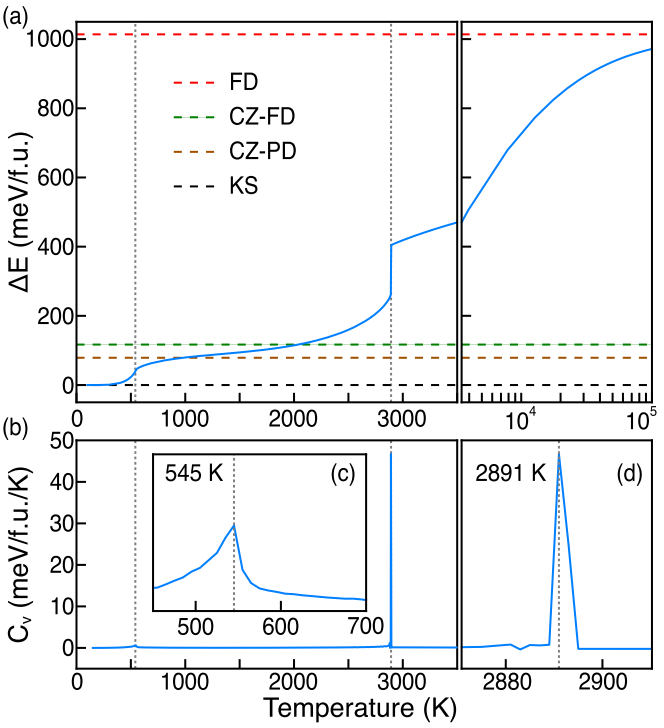

FIG. 2. (a) Variation of the energy (ΔE) and (b) heat capacity C_v obtained from MC simulations as functions of temperature. In panel (a), the temperature scale is linear up to 3500 K and logarithmic thereafter. Two phase transitions are identified by gray dotted vertical lines. The relative energies of the KS, CZ-PD, CZ-FD, and FD phases, computed with CE, are indicated by black, brown, green, and red dashed lines, respectively. Panels (c) and (d) show the two phase transitions, around 545 and 2891 K, respectively, in detail.

observables were measured by averaging over 10^5 passes. Starting from a completely disordered structure at 10^5 K, the system was slowly cooled down to 100 K by a simulated annealing technique. Smaller temperature steps were used in the vicinity of the phase transition regions.

III. RESULTS AND DISCUSSION

A. Order-disorder phase transitions

By combining a ternary CE with MC simulations, the energy E can be calculated as a function of temperature. Since KS is the most stable structure of CZTS at $T = 0$ K, its energy (also obtained from CE) is chosen as the reference, and we focus on the energy difference ΔE with respect to KS. The dependence of ΔE on temperature is shown in Fig. 2(a).

At temperatures below 300 K, the energy of the system still almost coincides with the energy of KS (shown by the black dashed horizontal line). As the temperature increases, the energy curve shows a smooth transition, denoting a second order phase transition, around 500 K and a sharp discontinuity close to 2900 K. The ΔE values for the CZ-PD, CZ-FD and FD phases (computed from CE) are indicated by dashed horizontal lines in brown, green, and red, respectively. The ΔE values of CZ-PD and CZ-FD lie relatively close to each other and the system only enters this regime between the two phase transitions. Until this point, the disorder is restricted to the Cu-Zn sublattice and the probability of cation exchanges with Sn atoms is very low owing to the large chemical and size mismatch between the Cu/Zn and Sn atoms. The ΔE value of the FD phase is only reached at extremely high temperatures.

The heat capacity is obtained as the derivative of the energy with respect to temperature and is shown in Fig. 2(b). Two peaks corresponding to phase transitions occur at 545 and 2891 K. The first phase transition temperature, corresponding to Cu-Zn disorder, is in very good agreement with the reported experimental values of 533 ± 10 K and 552 K [8,18,27]. In contrast, the second transition temperature (2891 K) is overestimated in comparison to experimental observations (1150 K) [17,28]. Four possible reasons for this discrepancy have been identified. First, the vibrational entropy [47,48] is

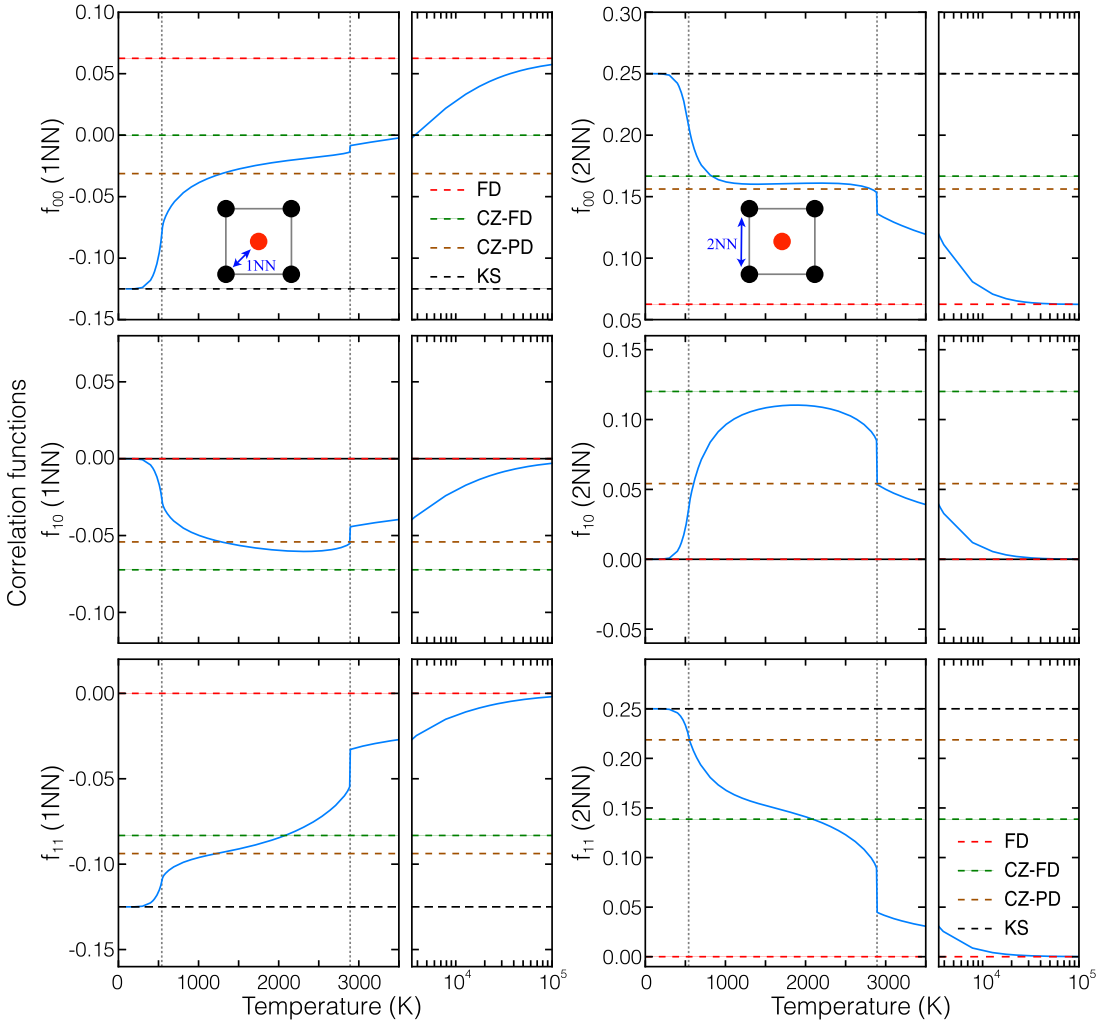

FIG. 3. The temperature evolution of the different pair-correlation functions (f00, f10, and f11) corresponding to 1NN and 2NN in CZTS as obtained from the MC simulations (solid blue curves). The corresponding values for the KS, CZ-PD, CZ-FD, and FD phases of CZTS are represented as black, brown, green, and red dashed lines, respectively. Phase transitions are identified by the changes of slope close to 545 and 2891 K.

neglected in our calculations. Second, the possible formation of vacancies is not taken into account and this becomes more important at higher temperatures. Third, the CZTS samples grown in experiments are often off-stoichiometric, which is not accounted for in our simulations. Last but not least, the errors on the CE energies are larger for the microstates with higher energies (see Fig. 5 in the Appendix), which become prevalent at higher temperatures in the MC simulation.

B. Phase identification from correlation functions

To understand the nature of the disorder observed in the MC simulations, we also analyze the temperature evolution of the pair-correlation functions (f00, f10, and f11) corresponding to the clusters (1NN and 2NN) included in the simulations (see Appendix). These six functions are shown as solid blue lines in Fig. 3 . The sign of their second-order derivative changes before and after both phase transitions, and a discontinuity is present at the second phase transition. The values of the corresponding pair-correlation functions for KS and the different disordered phases CZ-PD, CZ-FD, and FD are indicated by dashed horizontal lines in black, brown, green, and red, respectively.

When comparing the correlation functions of the disordered phases to the temperature-dependent correlation functions obtained from MC, we observe that at very low temperature, below 300 K, the correlation functions coincide with the correlation functions of KS (black dashed line). As the temperature increases, the MC correlation functions move towards the values of CZ-FD (green dashed line), most clearly observed in f10 (1NN and 2NN). After the second phase transition, the curves move towards the values of FD (red dashed line) at very high temperatures. At this stage, the entropy factor is high enough for exchanges to occur within the entire cation sublattice, including the Sn, hence leading to a full disorder in all cationic sites. The first phase transition is hence a transition from KS towards a CZ-FD phase, in contrast to earlier claims suggesting the involvement of a CZ-PD phase (brown dashed line) [5]. This analysis hence indicates complete disorder in the 2*a*, 2*c*, and 2*d* sites, in agreement with recent high-resolution neutron diffraction experiments [14]. We thus resolve the longstanding confusion on the nature of disorder in CZTS, rejecting the hypothesis of disorder only in the 2*c* and 2*d* sites, which corresponds to the CZ-PD phase.

IV. CONCLUSION

In this study we used a theoretical approach, combining ternary cluster expansion and Monte Carlo simulations to resolve the nature of the cation disorder in CZTS.

In the MC simulations, we observe two phase transitions. The system evolves from the KS structure via a phase with full disorder in the Cu and Zn ions among the 2*a*, 2*c*, and 2*d* Wyckoff sites to a phase including also disorder in the Sn ions. The previous interpretation of Cu-Zn disorder being restricted to the 2*c* and 2*d* sites thus seems incorrect. From the heat capacity we predict the low-temperature phase transition at 545 K, in very good agreement with experimental values. The temperature of the second transition, to full cationic disorder, is, however, overestimated due to limitations in the applied approach. Obtaining an accurate description at high temperature would probably require one to take into account the vibrational entropy and the possible formation of vacancies in the anion substructure, as well as to improve our CE model.

The present understanding could also help to further investigate nonstoichiometric CZTS (especially Cu-poor) compounds for which the efficiency is experimentally found to be higher than for stoichiometric CZTS.

ACKNOWLEDGMENTS

S.P.R. would like to thank the Fonds de la Recherche Scientifique (F.R.S.-FNRS), Belgium for financial support through a FRIA grant. G.-M.R. is grateful to the F.R.S.-FNRS for the financial support. A.M. and G.-M.R. would like to acknowledge funding from the Walloon Region (DGO6) through the CZTS project of the "Plan Marshall 2.vert" program. Computational resources have been provided by the supercomputing facilities of the Université catholique de Louvain (CISM/UCL) and the Consortium des Equipements de Calcul Intensif en Fédération Wallonie Bruxelles (CECI) funded by the Fonds de la Recherche Scientifique de Belgique (F.R.S.-FNRS). The authors would like to thank Anton Van der Ven for useful discussions on cluster expansion and Monte Carlo methods and Bruno Bertrand for discussions on CZTS.

APPENDIX A: EFFECT OF *U* ON THE ENERGETICS

As a starting point of the present study, we investigated the effect of U on the energetics of the different possible atomic arrangements of CZTS. To this end, we considered 11 different CZTS structures composed of 8, 16, and 24 atoms per unit cell. For each of these, we calculated the total energies with PBE, PBE+U, and HSE06 [49] as shown in Table I. Taking HSE results as a reference in terms of quality of the calculations, we found that there is no significant change with PBE+U compared to the standard PBE functional. The mean absolute error (MAE) of PBE+U is 3.3 meV/f.u. when compared to HSE while it is 5.1 meV/f.u. with PBE. The present study could have been performed using simply the latter. Nevertheless, the use of PBE+U was considered to be important for future work

TABLE I. Comparison of the energy difference with respect to KS (ΔE) for various structures computed within PBE, PBE+U, and HSE. For each structure, the space group and the number of atoms in the unit cell are indicated.

		ΔE (meV/f.u.)		
Space group	N_{atoms}	PBE	PBE+U	HSE
$I\bar{4}$	8	0.0	0.0	0.0
$I\bar{4}2m$	8	17.6	26.0	24.7
$P\bar{4}2m$	8	28.9	43.1	34.6
$P\bar{4}2c$	16	1.1	7.1	5.0
$C2$	16	10.6	13.4	16.5
$I\bar{4}2m$	16	23.1	30.4	29.2
$P\bar{4}2c$	16	25.9	33.1	33.6
$P222$	24	11.0	12.8	20.6
$I\bar{4}$	24	14.0	17.7	19.0
$I\bar{4}$	24	14.2	21.2	12.2
$I\bar{4}2m$	24	24.2	29.3	27.8

TABLE II. Cluster figures and the corresponding reduced coordinates, multiplicity, decoration, and ECIs obtained from CZTS CE of energy.

Cluster figure	Reduced coordinates	Multiplicity	Decoration	ECI (meV)
Empty		1		–27783.55
Point	(1,1,1)	4	0	0.00
	(1,1,1)	4	1	0.00
Pair (1NN)	(1/2,1,1/2),(0,1,0)	24	0,0	144.74
	(1/2,1,1/2),(0,1,0)	48	1,0	130.45
	(1/2,1,1/2),(0,1,0)	24	1,1	127.01
Pair (2NN)	(1/2,1/2,1),(1/2,1/2,0)	12	0,0	9.30
	(1/2,1/2,1),(1/2,1/2,0)	24	1,0	5.64
	(1/2,1/2,1),(1/2,1/2,0)	12	1,1	–0.80

in order to obtain an accurate description of the electronic properties [39].

APPENDIX B: CLUSTER EXPANSION

A configuration σ with N lattice sites can be represented by a vector of occupation variables such as $\sigma = \{\sigma_1, \sigma_2, \ldots, \sigma_N\}$, where each variable denotes the type of atom occupying lattice site i. In such an alloy, where site i can host M_i components, σ_i can take any value between 0 and $M_i - 1$. Let α be a group of n lattice sites, and $n = 1, 2, 3, \ldots$ indicates a single site, pair cluster, triplet cluster, and so on. The cluster function Π can then be defined as

$$\Pi^s_\alpha = \prod_{i\in\alpha} f_{s_i}(\sigma_i), \tag{B1}$$

where $f_{s_i}(\sigma_i)$ are called point functions. The vector $s = \{s_1, s_2, \ldots, s_n\}$ is called a "decoration", which specifies the type of point function associated with each site in the cluster α. The values for s_i range from 0 to $M_i - 2$. Hence, for a ternary system, it can be either 0 or 1.

In the present case, we consider disorder in all the cationic sites without any restrictions. Since there are three active components, the occupation variables are $\sigma \in \{0 : \mathrm{Cu}, 1 : \mathrm{Zn}, 2 : \mathrm{Sn}\}$. The point functions f_0 and f_1 to describe this three-component system are defined as

$$f_0 = -\cos\left(\frac{2}{3}\pi\sigma_i\right), \tag{B2}$$

$$f_1 = -\sin\left(\frac{2}{3}\pi\sigma_i\right). \tag{B3}$$

Hence the computed point functions $\{f_0, f_1\}$ corresponding to each of the species are (Cu $= \{-1,0\}$, Zn $= \{1/2, -\sqrt{3}/2\}$, and Sn $= \{1/2, \sqrt{3}/2\}$). By averaging Π^s_α over all the symmetrical equivalent clusters of the lattice, the correlation function $\bar{\Pi}^s_\alpha$ is obtained. A property such as the energy (E) that depends on the lattice configuration can be expanded using the CE technique as

$$E^{\mathrm{CE}}(\sigma) = J_0 + \sum_\alpha \sum_s m^s_\alpha J^s_\alpha \bar{\Pi}^s_\alpha(\sigma), \tag{B4}$$

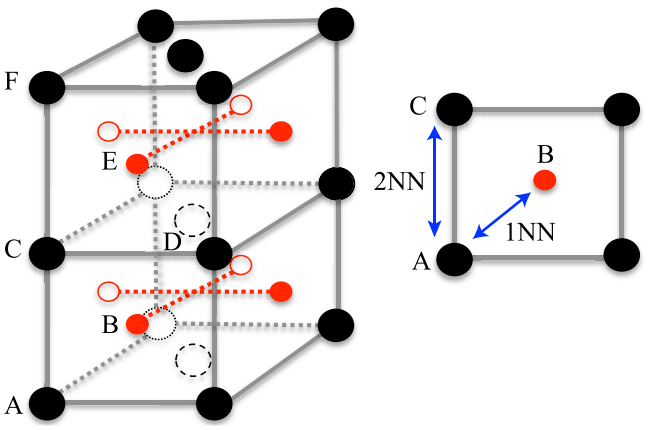

FIG. 4. A schematic of a 16-atom tetragonal unit cell indicating the relevant pair cluster interactions that are involved in the CE of energies in CZTS.

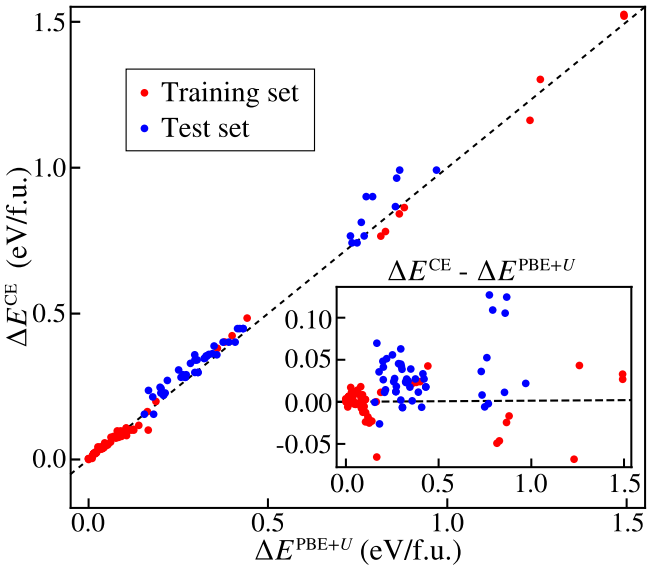

FIG. 5. Comparison of energy difference with respect to KS (in eV/f.u.) for the 70 structures of the training set (red dots) and the 50 structures of the test set (blue dots) computed within the CE (ΔE^{CE}) and within PBE+U ($\Delta E^{\mathrm{PBE}+U}$). The inset shows the error ($\Delta E^{\mathrm{CE}} - \Delta E^{\mathrm{PBE}+U}$ in eV/f.u.) made using the CE as a function of the PBE+U energy difference.

where m_α^s is the multiplicity factor indicating the number of symmetrically equivalent clusters of type α (with a decoration s) per lattice site and J_α^s is the configuration-independent Ising-type interaction called effective cluster interaction (ECI). J_0 is the ECI of the empty cluster.

Based on a least-squares fit of the PBE+U energies of a set of 70 structures, we obtained the ECIs shown in Table II (see Ref. [50]). We also consider a test set of 50 randomly selected structures to check the validity of the CE. All the structures considered here (both for the training and test sets) have the stoichiometric atomic composition of 50% Cu, 25% Zn, and 25% Sn.

The CE with the lowest cross-validation score (22.96 meV/f.u.) consists of only pair interactions involving 1NN and 2NN, as shown in Fig. 4. For each of the clusters, the product of point functions denotes the cluster function for a decoration s. Their average gives the correlation function, which can be represented as f_0f_0 (f00), f_0f_1 (f01), f_1f_0 (f10), and f_1f_1 (f11). The f01 and f10 are usually averaged, and we simply refer to the average as f10.

In Fig. 5, we compare the energy difference with respect to KS (in eV/f.u.) for the 70 structures of the training set (red dots) and the 50 structures of the test set (blue dots) computed within the CE (ΔE^{CE}) and within PBE+U ($\Delta E^{\mathrm{PBE}+U}$). The agreement is very good. The error made using this CE can be measured by the difference between the relative energies with respect to KS computed within the CE (ΔE^{CE}) and with an explicit PBE+U calculation ($\Delta E^{\mathrm{PBE}+U}$). It is reported in the inset of Fig. 5 as a function of $\Delta E^{\mathrm{PBE}+U}$. We note that the error tends to increase as the relative energies with respect to KS get larger. The maximum and mean absolute errors obtained for the training set are 68.2 and 12.4 meV/f.u., respectively, while they are 127.0 and 33.0 meV/f.u., respectively, for the test set.

[1] C. Breyer, D. Bogdanov, A. Gulagi, A. Aghahosseini, L. S. Barbosa, O. Koskinen, M. Barasa, U. Caldera, S. Afanasyeva, M. Child *et al.*, Prog. Photovolt. Res. Appl. **25**, 727 (2017).

[2] M. A. Green, Y. Hishikawa, W. Warta, E. D. Dunlop, D. H. Levi, J. Hohl-Ebinger, and A. W. Ho-Baillie, Prog. Photovol. Res. Appl. **25**, 668 (2017).

[3] W. Wang, M. T. Winkler, O. Gunawan, T. Gokmen, T. K. Todorov, Y. Zhu, and D. B. Mitzi, Adv. Energy Mater. **4**, 1301465 (2014).

[4] B. Shin, O. Gunawan, Y. Zhu, N. A. Bojarczuk, S. J. Chey, and S. Guha, Prog. Photovolt. Res. Appl. **21**, 72 (2013).

[5] S. Bourdais, C. Choné, B. Delatouche, A. Jacob, G. Larramona, C. Moisan, A. Lafond, F. Donatini, G. Rey, S. Siebentritt *et al.*, Adv. Energy Mater. **6**, 1502276 (2016).

[6] I. Olekseyuk, I. Dudchak, and L. Piskach, J. Alloys Compd. **368**, 135 (2004).

[7] M. Dimitrievska, A. Fairbrother, E. Saucedo, A. Pérez-Rodríguez, and V. Izquierdo-Roca, Sol. Energy Mater. Sol. Cells **149**, 304 (2016).

[8] J. J. Scragg, J. K. Larsen, M. Kumar, C. Persson, J. Sendler, S. Siebentritt, and C. Platzer Björkman, Phys. Status Solidi B **253**, 247 (2016).

[9] T. Gokmen, O. Gunawan, T. K. Todorov, and D. B. Mitzi, Appl. Phys. Lett. **103**, 103506 (2013).

[10] S. Chen, X. G. Gong, A. Walsh, and S.-H. Wei, Phys. Rev. B **79**, 165211 (2009).

[11] A. Walsh, S. Chen, S.-H. Wei, and X.-G. Gong, Adv. Energy Mater. **2**, 400 (2012).

[12] S. Chen, A. Walsh, X.-G. Gong, and S.-H. Wei, Adv. Mater. **25**, 1522 (2013).

[13] S. Chen, J.-H. Yang, X.-G. Gong, A. Walsh, and S.-H. Wei, Phys. Rev. B **81**, 245204 (2010).

[14] C. J. Bosson, M. T. Birch, D. P. Halliday, K. S. Knight, A. S. Gibbs, and P. D. Hatton, J. Mater. Chem. A **5**, 16672 (2017).

[15] M. Valentini, C. Malerba, F. Menchini, D. Tedeschi, A. Polimeni, M. Capizzi, and A. Mittiga, Appl. Phys. Lett. **108**, 211909 (2016).

[16] M. Quennet, A. Ritscher, M. Lerch, and B. Paulus, J. Solid State Chem. **250**, 140 (2017).

[17] S. Schorr, Sol. Energy Mater. Solar Cells **95**, 1482 (2011).

[18] J. J. Scragg, L. Choubrac, A. Lafond, T. Ericson, and C. Platzer-Björkman, Appl. Phys. Lett. **104**, 041911 (2014).

[19] J. M. Skelton, A. J. Jackson, M. Dimitrievska, S. K. Wallace, and A. Walsh, APL Mater. **3**, 041102 (2015).

[20] S. P. Ramkumar, Y. Gillet, A. Miglio, M. J. van Setten, X. Gonze, and G.-M. Rignanese, Phys. Rev. B **94**, 224302 (2016).

[21] M. Dimitrievska, F. Boero, A. P. Litvinchuk, S. Delsante, G. Borzone, A. Perez-Rodriguez, and V. Izquierdo-Roca, Inorg. Chem. **56**, 3467 (2017).

[22] M. Paris, G. Larramona, P. Bais, S. Bourdais, A. Lafond, C. Choné, C. Guillot-Deudon, B. Delatouche, C. Moisan, and G. Dennler, J. Phys. Chem. C **119**, 26849 (2015).

[23] M. Paris, L. Choubrac, A. Lafond, C. Guillot-Deudon, and S. Jobic, Inorg. Chem. **53**, 8646 (2014).

[24] S. Schorr, H.-J. Hoebler, and M. Tovar, Eur. J. Mineral. **19**, 65 (2007).

[25] A. Lafond, L. Choubrac, C. Guillot-Deudon, P. Fertey, M. Evain, and S. Jobic, Acta Crystallogr. Sect. B **70**, 390 (2014).

[26] J. Paier, R. Asahi, A. Nagoya, and G. Kresse, Phys. Rev. B **79**, 115126 (2009).

[27] A. Ritscher, M. Hoelzel, and M. Lerch, J. Solid State Chem. **238**, 68 (2016).

[28] S. Schorr and G. Gonzalez-Aviles, Phys. Status Solidi A **206**, 1054 (2009).

[29] S. Shang, Y. Wang, G. Lindwall, N. R. Kelly, T. J. Anderson, and Z.-K. Liu, J. Phys. Chem. C **118**, 24884 (2014).

[30] A. Zunger, S.-H. Wei, L. G. Ferreira, and J. E. Bernard, Phys. Rev. Lett. **65**, 353 (1990).

[31] K. Yu and E. A. Carter, Chem. Mater. **28**, 864 (2016).

[32] J. M. Sanchez, F. Ducastelle, and D. Gratias, Physica A (Amsterdam) **128**, 334 (1984).

[33] P. J. Van Laarhoven and E. H. Aarts, in *Simulated Annealing: Theory and Applications* (Springer, New York, 1987).

[34] P. Zawadzki, A. Zakutayev, and S. Lany, Phys. Rev. Appl. **3**, 034007 (2015).

[35] G. Kresse and J. Furthmüller, Comput. Mater. Sci. **6**, 15 (1996).

[36] P. E. Blöchl, Phys. Rev. B **50**, 17953 (1994).

[37] J. P. Perdew, K. Burke, and M. Ernzerhof, Phys. Rev. Lett. **77**, 3865 (1996).
[38] S. L. Dudarev, G. A. Botton, S. Y. Savrasov, C. J. Humphreys, and A. P. Sutton, Phys. Rev. B **57**, 1505 (1998).
[39] S. Botti, D. Kammerlander, and M. A. Marques, Appl. Phys. Lett. **98**, 241915 (2011).
[40] J. Vidal, S. Botti, P. Olsson, J.-F. Guillemoles, and L. Reining, Phys. Rev. Lett. **104**, 056401 (2010).
[41] C. Persson and A. Zunger, Appl. Phys. Lett. **87**, 211904 (2005).
[42] C. Persson, Appl. Phys. Lett. **93**, 072106 (2008).
[43] S.-H. Han, C. Persson, F. S. Hasoon, H. A. Al-Thani, A. M. Hermann, and D. H. Levi, Phys. Rev. B **74**, 085212 (2006).
[44] From the standpoint of the energetics of the different structures, the value of U does not affect the results significantly (see Table I in the Appendix). The present study could have been performed using simply the PBE approximation.
[45] A. van de Walle and G. Ceder, J. Phase Equilib. **23**, 348 (2002).
[46] A. van de Walle, Calphad **33**, 266 (2009).
[47] A. Van De Walle and G. Ceder, Rev. Mod. Phys. **74**, 11 (2002).
[48] A. van de Walle, JOM **65**, 1523 (2013).
[49] A. V. Krukau, O. A. Vydrov, A. F. Izmaylov, and G. E. Scuseria, J. Chem. Phys. **125**, 224106 (2006).
[50] S. P. Ramkumar, Ab-initio study of structural, thermodynamical, vibrational and electronic properties of CZTS, Ph.D. thesis, UC Louvain, 2017.